

# MULTI-MODAL IMAGE PROCESSING BASED ON COUPLED DICTIONARY LEARNING

Pingfan Song\* Miguel R. D. Rodrigues\*

\* Department of Electronic and Electrical Engineering, University College London, UK

## ABSTRACT

In real-world scenarios, many data processing problems often involve heterogeneous images associated with different imaging modalities. Since these multimodal images originate from the same phenomenon, it is realistic to assume that they share common attributes or characteristics. In this paper, we propose a multi-modal image processing framework based on coupled dictionary learning to capture similarities and disparities between different image modalities. In particular, our framework can capture favorable structure similarities across different image modalities such as edges, corners, and other elementary primitives in a learned sparse transform domain, instead of the original pixel domain, that can be used to improve a number of image processing tasks such as denoising, inpainting, or super-resolution. Practical experiments demonstrate that incorporating multimodal information using our framework brings notable benefits.

**Index Terms**— multimodal image processing, coupled dictionary learning, joint sparse representation, denoising, inpainting, super-resolution

## 1. INTRODUCTION

In many practical application scenarios, it is common to image a certain scene using various sensors that yield different image modalities. For example, in remote sensing domain, it is typical to have various image modalities of earth observations, such as a panchromatic band version, a multispectral bands version, and an infrared (IR) band version [1, 2]. These different bands often exhibit similar textures, edges, corners, boundaries, or other salient features. In medical imaging domain, multi-contrast scans for the same underlying anatomy [3–5], such as simultaneous positron emission tomography (PET) / magnetic resonance imaging (MRI) scans, MRI T1/T2-weighted scans, also indicate strong correlation. In colorization [6] tasks, the output image has both chrominance channels and luminance channel which share consistent edges. These scenarios call for approaches that can capitalize on the availability of multiple image modalities of the same scene, object, or phenomenon to address interested image processing tasks.

This work was supported by the Royal Society International Exchange Scheme IE160348, by UCL Overseas Research Scholarship (UCL-ORS) and by China Scholarship Council (CSC).

A number of multimodal image processing approaches have also been proposed in the literature to capitalize on the availability of additional *guidance* or *side information* [7, 8], to aid the processing of target modalities, also referred as joint/collaborative image filtering [9–22]. Generally, the basic idea behind these approaches is that the structural details of the guidance image can be transferred to the target image. These approaches have been applied to multi-modal image denoising, super-resolution, classification, and more. However, these methods tend to introduce notable texture-copying artifacts, i.e. erroneous structure details that are not originally present in the target image because such methods typically fail to distinguish similarities from disparities between different image modalities.

In this paper, we propose a new multimodal image processing framework based on coupled dictionary learning. In particular, our model captures complex correlation between different modalities using joint sparse representations over a set of adaptive coupled dictionaries. This enables us to take into account both similarities and disparities of different modalities via considering their common and unique sparse representations which are obtained in learned sparse domains. This characteristic makes our approach robust to inconsistencies between the guidance and target images, as proper guidance information can be extracted from the guidance modality and then be incorporated in a task-specific formulation to aid the processing of the target modality. Moreover, due to the sparsity prior, our model also demonstrates better robustness than other competing methods in presence of noise.

## 2. MULTI-MODAL IMAGE DENOISING

We first present our coupled dictionary learning framework for multi-modal image denoising.

### 2.1. Data Model for Denoising

Consider a vectorized noisy image  $\mathbf{X}^{ns} \in \mathbb{R}^N$  of one modality and a corresponding registered clean vectorized guidance image  $\mathbf{Y} \in \mathbb{R}^N$  of different modality as side information. We first extract (overlapping) image patch pairs from this pair of multimodal images. In particular, let  $\mathbf{x}_i^{ns} = \mathbf{R}_i \mathbf{X}^{ns} \in \mathbb{R}^n$  denote the  $i$ -th noisy image patch extracted from  $\mathbf{X}^{ns}$  and let  $\mathbf{y}_i = \mathbf{R}_i \mathbf{Y} \in \mathbb{R}^n$  denote the corresponding  $i$ -th clean guidance image patch extracted from  $\mathbf{Y}$ , where the matrix  $\mathbf{R}_i$  is an  $n \times N$  binary matrix that extracts the  $i$ -th patch from the

image. Then, we propose a data model to capture the relationship – including similarities and disparities – between the two different modalities as follows:

$$\begin{aligned} \mathbf{x}_i^{ns} &= \Psi_c \mathbf{z}_i + \Psi \mathbf{u}_i + \epsilon, \\ \mathbf{y}_i &= \Phi_c \mathbf{z}_i + \Phi \mathbf{v}_i, \end{aligned} \quad (1)$$

where the sparse representation  $\mathbf{z}_i \in \mathbb{R}^K$  is common to both modalities, the sparse representation  $\mathbf{u}_i \in \mathbb{R}^K$  is specific to modality  $\mathbf{x}$ , while the sparse representation  $\mathbf{v}_i \in \mathbb{R}^K$  is specific to modality  $\mathbf{y}$ . In turn,  $\Psi_c$  and  $\Phi_c \in \mathbb{R}^{n \times K}$  are a pair of dictionaries associated with the common sparse representation  $\mathbf{z}_i$ , whereas  $\Psi$  and  $\Phi \in \mathbb{R}^{n \times K}$  are dictionaries associated with the specific sparse representations  $\mathbf{u}_i$  and  $\mathbf{v}_i$ , respectively. Note that the common sparse representation  $\mathbf{z}_i$  connects the patches of the two different modalities. The disparities between modalities  $\mathbf{x}$  and  $\mathbf{y}$  are distinguished by the sparse representations  $\mathbf{u}_i$  and  $\mathbf{v}_i$ , respectively. Finally,  $\epsilon \in \mathbb{R}^n$  denotes additive zero-mean and homogeneous white Gaussian noise with the standard deviation  $\sigma$ .

## 2.2. Coupled Image Denoising

Our coupled image denoising problem is addressed in two steps: coupled dictionary learning and reconstruction of the denoised image.

**Step 1: Coupled dictionary learning.** In this stage, given a set of training patch pairs  $\{\mathbf{x}_i^{ns}, \mathbf{y}_i\}$ , we aim to solve the following optimization problem:

$$\min_{\mathbf{D}, \alpha} \sum_i \left\| \begin{bmatrix} \mathbf{x}_i^{ns} \\ \mathbf{y}_i \end{bmatrix} - \begin{bmatrix} \Psi_c & \Psi & \mathbf{0} \\ \Phi_c & \mathbf{0} & \Phi \end{bmatrix} \begin{bmatrix} \mathbf{z}_i \\ \mathbf{u}_i \\ \mathbf{v}_i \end{bmatrix} \right\|_2 \text{ s.t. } \left\| \begin{bmatrix} \mathbf{z}_i \\ \mathbf{u}_i \\ \mathbf{v}_i \end{bmatrix} \right\|_0 \leq s_i, \forall i, \quad (3)$$

where,  $\mathbf{D}$  and  $\alpha$  represent all the dictionaries and sparse representations. The  $\ell_0$  term serves as the sparsity-inducing operation. The quadratic "data-fitting" term ensures that each pair of multimodal image patches is well approximated by their sparse representations with respect to the learned dictionaries. The coupled dictionary learning problems in (3) is a non-convex optimization problem. We solve it via an alternating optimization scheme that performs 1) sparse coding and 2) dictionary update alternatively. During the sparse coding stage, we fix all the dictionaries and obtain the sparse representations using orthogonal matching pursuit (OMP) algorithm [23], while during the dictionary updating stage, we fix the sparse codes and update the all the dictionaries using adapted K-SVD algorithm [24]. In our case, we stick to  $\ell_0$  penalty for the sparse coding as it usually leads to better denoising performance than  $\ell_1$  penalty, which is also observed in [25, 26].

**Step 2: Reconstruction.** In this stage, given the sparse codes  $\mathbf{z}_i, \mathbf{u}_i$ , the denoised image can be estimated from the noisy version by solving

$$\min_{\mathbf{X}} \mu \|\mathbf{X} - \mathbf{X}^{ns}\|_2^2 + \sum_i \|\mathbf{R}_i \mathbf{X} - (\Psi_c \mathbf{z}_i + \Psi \mathbf{u}_i)\|_2^2 \quad (4)$$

where,  $\mu$  trades off between the fidelity to the noisy version and the fidelity to the sparse estimation.<sup>1</sup> This leads immediately to a closed form solution

$$\mathbf{X} = \left( \mu \mathbf{I} + \sum_i \mathbf{R}_i^T \mathbf{R}_i \right)^{-1} \left( \mu \mathbf{X}^{ns} + \sum_i \mathbf{R}_i^T (\Psi_c \mathbf{z}_i + \Psi \mathbf{u}_i) \right). \quad (5)$$

## 3. MULTIMODAL IMAGE SUPER-RESOLUTION

We now present our coupled dictionary learning framework for multi-modal image super-resolution.

### 3.1. Data Model for Super-resolution

Similar to section 2.1, we consider a pair of vectorized low-resolution (LR) and high-resolution (HR) images  $\mathbf{X}^l \in \mathbb{R}^M$  and  $\mathbf{X}^h \in \mathbb{R}^N$  of one modality and a corresponding registered HR guidance image  $\mathbf{Y} \in \mathbb{R}^N$  of different modality as side information. In particular, let  $\mathbf{x}_i^l \in \mathbb{R}^m$  and  $\mathbf{x}_i^h \in \mathbb{R}^n$  denote the  $i$ -th LR/HR image patch pair extracted from  $\mathbf{X}^l$  and  $\mathbf{X}^h$  and let  $\mathbf{y}_i \in \mathbb{R}^n$  denote the corresponding  $i$ -th HR guidance image patch extracted from  $\mathbf{Y}$ . Then, based on the following two main assumptions: (1)  $\mathbf{x}_i^l$  and  $\mathbf{x}_i^h$  of the same modality share the same sparse representations with respect to their own dictionaries, which is also adopted by [27–29]; (2) a pair of registered image patches from different modalities  $\mathbf{x}_i^h$  and  $\mathbf{y}_i$  admit both identical and diverse sparse representations, we propose the data model (6) - (8) to capture the relationship across the LR/HR patches of a certain image modality along with the corresponding patch of another image modality.

$$\mathbf{x}_i^h = \Psi_c^h \mathbf{z}_i + \Psi^h \mathbf{u}_i, \quad (6)$$

$$\mathbf{x}_i^l = \Psi_c^l \mathbf{z}_i + \Psi^l \mathbf{u}_i, \quad (7)$$

$$\mathbf{y}_i = \Phi_c \mathbf{z}_i + \Phi \mathbf{v}_i, \quad (8)$$

where, similar to (1) and (2),  $\mathbf{z}_i \in \mathbb{R}^K$  is the common sparse representation, while  $\mathbf{u}_i \in \mathbb{R}^K$  and  $\mathbf{v}_i \in \mathbb{R}^K$  are the unique sparse representations.  $\Psi_c^h, \Psi_c^l$  and  $\Phi_c \in \mathbb{R}^{n \times K}$  are the dictionaries associated with  $\mathbf{z}_i$ , whereas  $\Psi^h, \Psi^l$  and  $\Phi \in \mathbb{R}^{n \times K}$  are dictionaries associated with  $\mathbf{u}$  and  $\mathbf{v}$ , respectively. Note that the sparse vectors  $\mathbf{z}_i$  and  $\mathbf{u}_i$  capture the relationship between the LR and HR patches of the same modality in (6) and (7). Moreover, the common sparse vector  $\mathbf{z}_i$  connects the various patches of the two different modalities in (6) - (8). The disparities between modalities are distinguished by the sparse vectors  $\mathbf{u}_i$  and  $\mathbf{v}_i$ .

### 3.2. Coupled Super Resolution (CSR)

Our coupled image super-resolution problem is addressed in 3 steps: coupled dictionary learning, coupled sparse coding and reconstruction of the HR image.

**Step 1: Coupled dictionary learning.** Given a set of training patch pairs  $\{\mathbf{x}_i^l, \mathbf{x}_i^h, \mathbf{y}_i\}$ , we solve the following optimization

<sup>1</sup>For  $\mu = 0$ , this expression just represents the average of the denoised image patches on the overlapping areas, leading to a purified image.

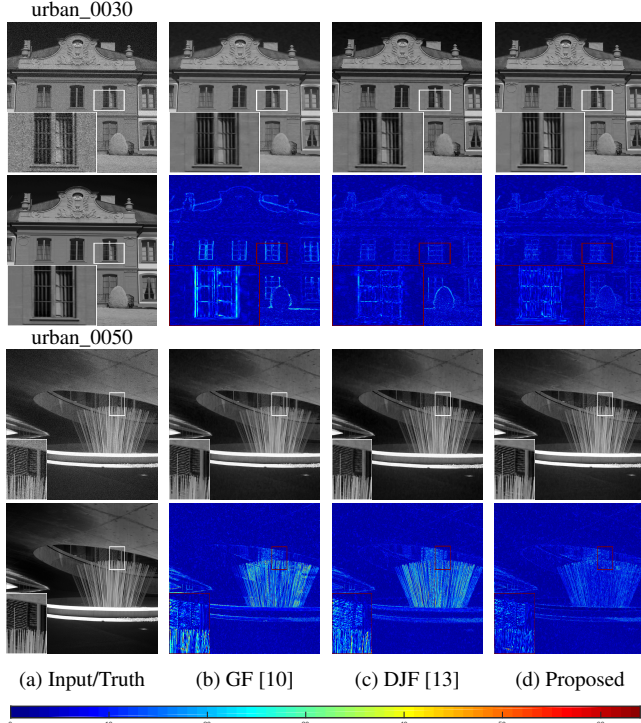


**Fig. 1.** Multimodal image denoising for near-infrared images ( $\sigma = 16$ ). For each scene, the first row is the noisy input and denoised results and the second row is the ground truth and corresponding error map for each approach.

problems (9) to train a group of dictionaries.

$$\min_{\mathbf{D}, \alpha} \sum_i \left\| \begin{bmatrix} \mathbf{x}_i^h \\ \mathbf{x}_i^l \\ \mathbf{y}_i \end{bmatrix} - \begin{bmatrix} \Psi_c^h & \Psi^h & \mathbf{0} \\ \Psi_c^l & \Psi^l & \mathbf{0} \\ \Phi & \mathbf{0} & \Phi \end{bmatrix} \begin{bmatrix} \mathbf{z}_i \\ \mathbf{u}_i \\ \mathbf{v}_i \end{bmatrix} \right\|_2^2 \quad \text{s.t.} \quad \left\| \begin{bmatrix} \mathbf{z}_i \\ \mathbf{u}_i \\ \mathbf{v}_i \end{bmatrix} \right\|_0 \leq s_i, \forall i, \quad (9)$$

where the  $\ell_2$  norm promotes the data fidelity; the  $\ell_0$  pseudo-norm promotes sparsity for the sparse codes;  $\mathbf{D}$  and  $\alpha$  represent all the dictionaries and sparse representations.

**Step 2: Coupled sparse coding.** Given a new LR testing image and a corresponding registered HR guidance image as side information. We extract (overlapping) image patch pairs from these two modalities. Then we solve a sparse coding problem, similar to (9) but with fixed dictionaries learned from Step 1 and involving no  $\mathbf{x}_i^h$  and  $[\Psi_c^h, \Psi^h]$ .

**Step 3: Reconstruction.** Finally, we can obtain each estimated HR patch  $\mathbf{x}_i^h$  of the target image from the HR dictionaries  $[\Psi_c^h, \Psi^h]$  and sparse codes  $\mathbf{z}_i$  and  $\mathbf{u}_i$  as follows

$$\mathbf{x}_i^h = \Psi_c^h \mathbf{z}_i + \Psi^h \mathbf{u}_i. \quad (10)$$

Once all the HR patches are recovered, they are integrated into a whole image by averaging on the overlapping areas.

#### 4. MULTIMODAL IMAGE INPAINTING

We finally introduce our framework for the multi-modal image inpainting task, a scenario where one needs to inpaint im-

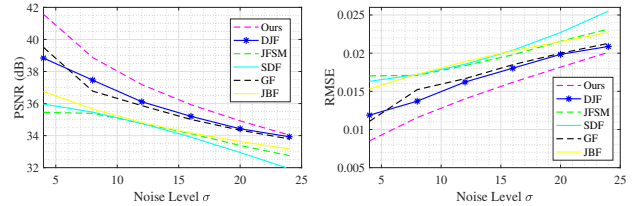


**Fig. 2.** Multimodal image denoising in terms of PSNR and RMSE with respect to different noise levels. We compare our approach with state-of-the-art joint image filtering approaches, JBF [9], GF [10], SDF [11], JFSM [12] and DJF [13].

ages with some small holes resulting from missing pixels. To deal with unobserved data, we introduce a binary mask  $\mathbf{M}_i$  for  $i$ -th patch, which is defined as a diagonal matrix whose value on the  $j$ -th entry of the diagonal is 1 if the pixel  $\mathbf{x}_i^h[j]$  is observed and 0 otherwise, similar to [26]. Then, we relate each corrupted image patch  $\mathbf{x}_i^l$  with the original image patch  $\mathbf{x}_i^h$  by a mask  $\mathbf{M}_i$ , as  $\mathbf{x}_i^l = \mathbf{M}_i \mathbf{x}_i^h$ . Similarly, there also exist dictionaries  $\Psi_{ci}^l = \mathbf{M}_i \Psi_c^h$ ,  $\Psi_i^l = \mathbf{M}_i \Psi_i^h$  for the  $i$ -th corrupted patch. Thus, the inpainting data model is identical to the super-resolution model in (6) - (8). We can still use (9) - (10) to solve the multi-modal inpainting problem, except no need to learn  $[\Psi_c^l, \Psi^l]$  from  $\mathbf{x}_i^l$  (since  $\mathbf{M}_i$  is known).

#### 5. EXPERIMENTS

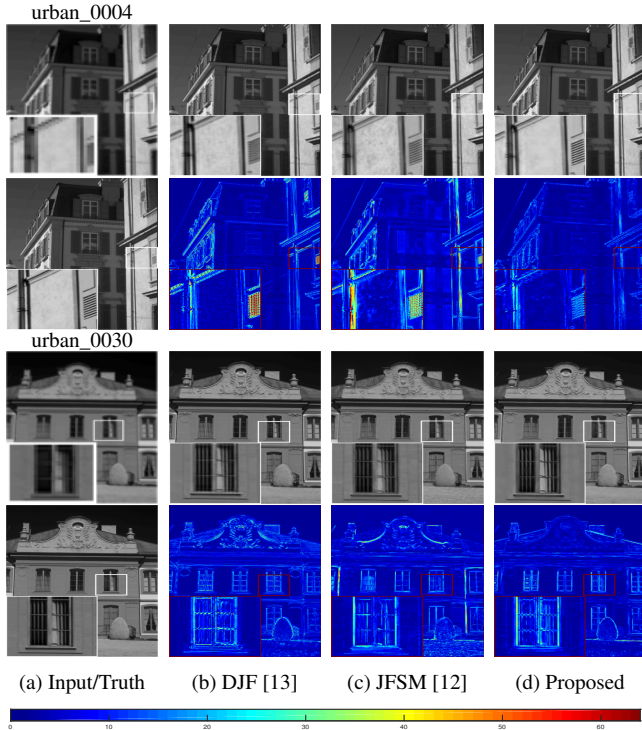
We now present a series of experiments to validate the effectiveness of the proposed multimodal image processing approaches. The dataset is from the EPFL infrared/RGB image database<sup>2</sup>. Each pair of near-infrared/RGB images in the dataset has been registered with each other. The target modality is near-infrared and the guidance modality is RGB. The image pairs are randomly separated into two disjointed groups: training group and testing group. The training image pairs lead to a training dataset consisting of 15000 image patch pairs of  $8 \times 8$  pixels. For denoising experiments, we add zero-mean white Gaussian noise with different standard deviations  $\sigma = [4, 8, 12, 16, 20, 24]$  into the near-infrared images to generate the noisy versions. For super-resolution experiments, we blur and downsample each HR near-infrared image by a factor, e.g.,  $4 \times$ , using the MATLAB "imresize" function to generate corresponding LR versions, similar to [27, 28]. We compare our approach with state-of-the-art joint image filtering approaches such as [9–12] and deep learning based approach [13]. The same guidance images as in our approach are leveraged by these comparison approaches as well. We adopt the Peak Signal to Noise Ratio (PSNR), the Root Mean square error (RMSE), and the Structure SIMilarity (SSIM) index [30] as the image quality evaluation metrics which are commonly used in the image processing literature.

Figure 1 demonstrates the visual quality of the purified

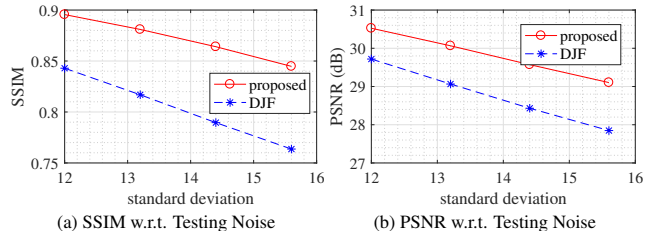
<sup>2</sup>[http://ivrl.epfl.ch/supplementary\\_material/cvpr11/](http://ivrl.epfl.ch/supplementary_material/cvpr11/)

**Table 1.** Multimodal image super-resolution for near-infrared images ( $4\times$  upscaling)

	Bicubic		JBF [9]		GF [10]		SDF [11]		DJF [13]		JFSM [12]		Proposed	
	SSIM	PSNR	SSIM	PSNR	SSIM	PSNR	SSIM	PSNR	SSIM	PSNR	SSIM	PSNR	SSIM	PSNR
urban_0004	0.9029	25.93	0.9359	28.47	0.9391	28.75	0.9066	26.82	0.9789	31.02	0.9721	30.86	<b>0.9811</b>	<b>34.14</b>
urban_0006	0.9458	30.89	0.9311	32.10	0.9400	32.66	0.8918	30.60	<b>0.9894</b>	36.04	0.9741	32.86	0.9868	<b>36.79</b>
urban_0017	0.9527	30.45	0.9172	31.11	0.9205	31.32	0.9281	30.72	<b>0.9815</b>	34.18	0.9500	32.85	0.9777	<b>35.27</b>
urban_0018	0.9298	25.19	0.9308	27.59	0.9251	27.70	0.9196	26.09	<b>0.9888</b>	30.72	0.9774	30.80	0.9874	<b>33.01</b>
urban_0020	0.9577	28.03	0.9523	30.67	0.9494	30.69	0.9505	29.09	<b>0.9915</b>	33.60	0.9797	32.61	0.9893	<b>36.66</b>
urban_0026	0.8704	26.27	0.8627	26.82	0.8571	26.89	0.8558	26.61	0.9397	29.21	0.9332	28.97	<b>0.9482</b>	<b>30.35</b>
urban_0030	0.8401	26.54	0.8476	27.58	0.8383	27.59	0.8415	27.21	0.9345	31.27	0.9064	30.56	<b>0.9443</b>	<b>32.71</b>
urban_0050	0.9434	26.65	0.9099	27.32	0.9116	27.35	0.9207	27.07	0.9616	28.58	0.9251	27.58	<b>0.9663</b>	<b>29.37</b>
average	0.9179	27.49	0.9109	28.96	0.9101	29.12	0.9018	28.03	0.9707	31.83	0.9522	30.89	<b>0.9726</b>	<b>33.54</b>

**Fig. 3.** Multimodal image super-resolution for near-infrared images ( $4\times$  upscaling). For each scene, the first row is the LR input and SR results and the second row is the ground truth and corresponding error map for each approach.

infrared images, as well as the corresponding error maps. As shown in the figure, our approach substantially attenuates the noise, reliably reserves image sharp details and suppresses artifacts. Therefore, the purified near-infrared images by our approach are cleaner and more visually plausible than the reconstruction by the competing approaches. The visual quality is also demonstrated by the error maps where the denoised near-infrared images using our approach exhibit the least residual for different noise levels in comparison with the competing methods. In particular, it can be observed that our approach also outperforms deep learning based approach DJF [13]. We believe that the good robustness and stability is due to sparsity priors exploited by our model. The average PSNR and average RMSE results for the multimodal image denoising task, shown in Figure 2, also confirm that

**Fig. 4.** Both the LR testing and training images are noisy for multimodal image SR ( $4\times$  upscaling), using DJF [13] and proposed approach. The standard deviation of the noise in the testing images ranges from 12 to 15.6.

our approach exhibits notable advantages over the competing methods.

Figure 3 compares the visual quality of the reconstructed HR near-infrared images and the corresponding error maps. It can be seen that our approach recovers more visually plausible images, exhibiting less error than the competing methods. Therefore, our reconstruction is more photo-realistic and visually appealing than the counterparts. Table 1 also confirm the significant advantage of the proposed approach over other state-of-the-art methods. Figure 4 shows the quantitative SR results for noisy LR input images of target modality. It is noticed that our algorithm demonstrates reasonable stability and robustness to noise, especially to strong noise. In contrast, DJF [13] is susceptible to noise and its performance degrades faster than ours.

## 6. CONCLUSION

This paper proposes a multimodal image processing framework based on coupled dictionary learning. The proposed scheme explicitly incorporates sparsity prior and cross-similarity prior in the data model to captures the similarities and disparities between different image modalities in a learned sparse feature domain in lieu of the original image domain. In this way, the proposed scheme can take better advantage of a guidance image modality to aid the processing of another different image modality in various tasks such as denoising, super-resolution. The experiments demonstrate that our framework achieves notable benefits with respect to the state-of-the-art, as well as outperforms deep-learning-based methods especially when the data is contaminated by noise.

## 7. REFERENCES

- [1] L. Gomez-Chova, D. Tuia, G. Moser *et al.*, “Multimodal classification of remote sensing images: a review and future directions,” *Proceedings of the IEEE*, vol. 103, no. 9, pp. 1560–1584, 2015.
- [2] L. Loncan, L. B. de Almeida, J. M. Bioucas-Dias *et al.*, “Hyperspectral pansharpening: A review,” *IEEE Geosci. Remote Sens. Mag.*, vol. 3, no. 3, pp. 27–46, 2015.
- [3] S. R. Cherry, “Multimodality in vivo imaging systems: twice the power or double the trouble?” *Annu. Rev. Biomed. Eng.*, vol. 8, pp. 35–62, 2006.
- [4] D. Townsend, “Multimodality imaging of structure and function,” *Physics in medicine and biology*, vol. 53, no. 4, p. R1, 2008.
- [5] C. Catana, A. R. Guimaraes, and B. R. Rosen, “PET and MR imaging: the odd couple or a match made in heaven?” *Journal of Nuclear Medicine*, vol. 54, no. 5, pp. 815–824, 2013.
- [6] A. Levin, D. Lischinski, and Y. Weiss, “Colorization using optimization,” in *ACM transactions on graphics (tog)*, vol. 23, no. 3. ACM, 2004, pp. 689–694.
- [7] F. Renna, L. Wang, X. Yuan *et al.*, “Classification and reconstruction of high-dimensional signals from low-dimensional features in the presence of side information,” *IEEE Trans. Inform. Theory*, vol. 62, no. 11, pp. 6459–6492, 2016.
- [8] J. F. Mota, N. Deligiannis, and M. R. Rodrigues, “Compressed sensing with prior information: Strategies, geometry, and bounds,” *IEEE Trans. Inform. Theory*, vol. 63, no. 7, 2017.
- [9] J. Kopf, M. F. Cohen, D. Lischinski *et al.*, “Joint bilateral up-sampling,” in *ACM Trans. Graph.*, vol. 26, no. 3. ACM, 2007, p. 96.
- [10] K. He, J. Sun, and X. Tang, “Guided image filtering,” *IEEE Trans. Pattern Anal. Mach. Intell.*, vol. 35, no. 6, pp. 1397–1409, 2013.
- [11] B. Ham, M. Cho, and J. Ponce, “Robust guided image filtering using nonconvex potentials,” *IEEE Trans. Pattern Anal. Mach. Intell.*, 2017.
- [12] X. Shen, Q. Yan, L. Xu *et al.*, “Multispectral joint image restoration via optimizing a scale map,” *IEEE Trans. Pattern Anal. Mach. Intell.*, vol. 37, no. 12, pp. 2518–2530, 2015.
- [13] Y. Li, J.-B. Huang, N. Ahuja *et al.*, “Deep joint image filtering,” in *Proc. Eur. Conf. Comput. Vision*. Springer, 2016, pp. 154–169.
- [14] Q. Zhang, X. Shen, L. Xu *et al.*, “Rolling guidance filter,” in *Proc. Eur. Conf. Comput. Vision*. Springer, 2014, pp. 815–830.
- [15] S. Wang, L. Zhang, Y. Liang *et al.*, “Semi-coupled dictionary learning with applications to image super-resolution and photo-sketch synthesis,” in *Proc. IEEE Conf. Comput. Vision Pattern Recog.* IEEE, 2012, pp. 2216–2223.
- [16] Y. T. Zhuang, Y. F. Wang, F. Wu *et al.*, “Supervised coupled dictionary learning with group structures for multi-modal retrieval,” in *Twenty-Seventh AAAI Conference on Artificial Intelligence*, 2013.
- [17] X. Liu, M. Song, D. Tao *et al.*, “Semi-supervised coupled dictionary learning for person re-identification,” in *Proc. IEEE Conf. Comput. Vision Pattern Recog.*, 2014, pp. 3550–3557.
- [18] X.-Y. Jing, X. Zhu, F. Wu *et al.*, “Super-resolution person re-identification with semi-coupled low-rank discriminant dictionary learning,” in *Proc. IEEE Conf. Comput. Vision Pattern Recog.*, 2015, pp. 695–704.
- [19] M. Dao, N. H. Nguyen, N. M. Nasrabadi *et al.*, “Collaborative multi-sensor classification via sparsity-based representation,” *IEEE Trans. Signal Process.*, vol. 64, no. 9, pp. 2400–2415, 2016.
- [20] S. Bahrampour, N. M. Nasrabadi, A. Ray *et al.*, “Multimodal task-driven dictionary learning for image classification,” *IEEE Trans. Image Process.*, vol. 25, no. 1, pp. 24–38, 2016.
- [21] N. Deligiannis, J. F. Mota, B. Cornelis *et al.*, “Multi-modal dictionary learning for image separation with application in art investigation,” *IEEE Trans. Image Process.*, vol. 26, no. 2, pp. 751–764, 2017.
- [22] N. Deligiannis, J. F. Mota, B. Cornelis *et al.*, “X-ray image separation via coupled dictionary learning,” in *IEEE Int. Conf. Image Process.* IEEE, 2016, pp. 3533–3537.
- [23] J. A. Tropp and A. C. Gilbert, “Signal recovery from random measurements via orthogonal matching pursuit,” *IEEE Trans. Inform. Theory*, vol. 53, no. 12, pp. 4655–4666, 2007.
- [24] M. Aharon, M. Elad, and A. Bruckstein, “K-svd: An algorithm for designing overcomplete dictionaries for sparse representation,” *IEEE Trans. Signal Process.*, vol. 54, no. 11, pp. 4311–4322, 2006.
- [25] J. Mairal, F. Bach, J. Ponce *et al.*, “Non-local sparse models for image restoration,” in *Proc. IEEE Int. Conf. Comput. Vision*. IEEE, 2009, pp. 2272–2279.
- [26] J. Mairal, F. Bach, J. Ponce *et al.*, “Sparse modeling for image and vision processing,” *Foundations and Trends® in Computer Graphics and Vision*, vol. 8, no. 2-3, pp. 85–283, 2014.
- [27] J. Yang, J. Wright, T. Huang *et al.*, “Image super-resolution as sparse representation of raw image patches,” in *Proc. IEEE Conf. Comput. Vision Pattern Recog.* IEEE, 2008, pp. 1–8.
- [28] J. Yang, J. Wright, T. S. Huang *et al.*, “Image super-resolution via sparse representation,” *IEEE Trans. Image Process.*, vol. 19, no. 11, pp. 2861–2873, 2010.
- [29] R. Zeyde, M. Elad, and M. Protter, “On single image scale-up using sparse-representations,” in *Curves and Surfaces*. Springer, 2010, pp. 711–730.
- [30] Z. Wang, A. C. Bovik, H. R. Sheikh *et al.*, “Image quality assessment: from error visibility to structural similarity,” *IEEE Trans. Image Process.*, vol. 13, no. 4, pp. 600–612, 2004.